The ferroelectric and cubic phases in BaTiO3 ferroelectrics are also antiferroelectric

Qingsong Zhang, Tahir Cagin, and William A. Goddard, III

PNAS 2006;103;14695-14700; originally published online Sep 25, 2006;
doi:10.1073/pnas.0606612103

The ferroelectric and cubic phases in $BaTiO_3$ ferroelectrics are also antiferroelectric

Qingsong Zhang, Tahir Cagin*, and William A. Goddard III†

Materials and Processes Simulation Center (MC 139-74), 1200 East California Boulevard, California Institute of Technology, Pasadena, CA 91125

Contributed by William A. Goddard III, August 1, 2006

Using quantum mechanics (QM, Density Functional Theory) we show that all four phases of barium titanate ($BaTiO_3$) have local Ti distortions toward ⟨111⟩ (an octahedral face). The stable rhombohedral phase has all distortions in phase (ferroelectric, FE), whereas higher temperature phases have antiferroelectric coupling (AFE) in one, two, or three dimensions (orthorhombic, tetragonal, cubic). This FE–AFE model from QM explains such puzzling aspects of these systems as the allowed Raman excitation observed for the cubic phase, the distortions toward ⟨111⟩ observed in the cubic phase using x-ray fine structure, the small transition entropies, the heavily damped soft phonon modes, and the strong diffuse x-ray scattering in all but the rhombohedral phase. In addition, we expect to see additional weak Bragg peaks at the face centers of the reciprocal lattice for the cubic phase. Similar FE–AFE descriptions are expected to occur for other FE materials. Accounting for this FE–AFE nature of these phases is expected to be important in accurately simulating the domain wall structures, energetics, and dynamics, which in turn may lead to the design of improved materials.

barium titanate | phase transition

Ferroelectric (FE) materials have broad applications in transducers, actuators, capacitors, and memories. Particularly well studied is $BaTiO_3$, which has rhombohedral (R), orthorhombic (O), tetragonal (T), and cubic (C) phases. However, the microscopic nature of the phases and transitions in $BaTiO_3$ remains uncertain. A popular model in history is the displacive model (1, 2), in which the equilibrium position of each Ti atom is in the middle of the oxygen octahedron for C, but displaced microscopically in the ⟨111⟩, ⟨011⟩, or ⟨001⟩ macroscopic polarization directions for the R, O, and T ferroelectric phases, respectively. However, this displacive model

- Predicts that first-order Raman excitation should vanish in the cubic phase due to the microscopic inversion symmetry, contradicting experiments (3).
- Contradicts the x-ray fine structure (XAFS) experiments (4) that show that the Ti atoms are displaced along various of the eight possible ⟨111⟩ directions in all phases.
- Does not explain the heavily damped but nonzero frequency for the soft modes at the C to T transition observed by infrared reflectivity (IR) experiments (5).
- Does not explain the strong diffuse x-ray scattering observed in all but the rhombohedral phase.

To explain these failures of the displacive model, a spontaneous symmetry breaking has been hypothesized to occur in these systems (6). Thus Berserker (7), Comes *et al.* (8) and Chaves *et al.* (9) introduced the order–disorder eight-site model (8OD), in which all Ti atoms are microscopically located in one of eight potential minima along the ⟨111⟩ directions for all crystal phases. As in the displacive model, 8OD assumes that the low temperature R phase has all Ti atoms distorted in the same direction. As temperature increases, 8OD assumes disorder in the polarization along one or more crystal directions, leading to greatly increased configurational entropy. However, 8OD

- Fails to predict the heavily damped low frequency phonon modes (soft modes) observed near the phase transitions by neutron scattering (10, 11), by IR (5) and by hyperRaman scattering (12).
- Would lead to the entropy changes of $\approx R\ln 2 = 5.76$ J/mol for the phase transitions, far larger than the observed entropy changes (≤ 0.52 J/mol) for each transition (8, 9). This observation forced the proponents of this model to postulate a 50- to 100-Å correlation length to reduce the entropy changes down to observed values.

Girshberg and Yacoby (13) proposed a model combining the displacive and order–disorder models. They developed this to explain mode softening near the FE phase transitions, and it was applied recently to $BaTiO_3$ (14) to explain the over damping (12) of the soft mode. The Girshberg–Yacoby theory showed that the existence of off-center displacements and their interaction with the soft modes could play a crucial role in explaining the properties of ferroelectric phase transitions.

Using the fundamental unit cell with one molecular unit, first-principles quantum mechanics (QM) calculations (15, 16) using the local density approximation to density functional theory (DFT) showed clearly that the Ti atoms are not in the central position in the cubic phase. These calculations also showed large volume dependence of the soft-mode potential surface and revealed the expected increase in total energies for the R, O, T, and C phases of $BaTiO_3$. Further phonon analysis (17, 18) on $BaTiO_3$ revealed two-dimensional character in the Brillouin zone, which corresponds to chains oriented along ⟨100⟩ directions of displaced Ti atoms. Such character had been found in $KNbO_3$ (19), a material with the same phase diagram as $BaTiO_3$. In addition, the $BaTiO_3$ phonon analysis showed that X point instability is slightly less unstable than Gamma point in $BaTiO_3$, implying a ferroelectric relaxation could lead to a lower-energy structure than an antiferroelectric relaxation.

On the other hand, the local structures and dynamics have also been studied in large supercells. Monte Carlo simulations (20) using an effective Hamiltonian based on the local density approximation DFT calculations found the correct sequence of transitions, leading to the suggestion that the phases have character intermediate between displacive and order–disorder. The crossover from a soft mode to an order–disorder dynamics was also found by a molecular dynamics (MD) study (21) using a nonlinear oxygen polarizability model. MD simulations (22, 23) using an effective Hamiltonian revealed the prevalence of local polar distortions with short-range chain-like correlations,

Author contributions: W.A.G. designed research; Q.Z. performed research; Q.Z. and T.C. analyzed data; and Q.Z. wrote the paper.

The authors declare no conflict of interest.

Abbreviations: FE, ferroelectric; R, rhombohedral; O, orthorhombic; T, tetragonal; C, cubic; XAFS, x-ray fine structure; IR, infrared reflectivity; 8OD, order–disorder eight-site model; QM, quantum mechanics; DFT, density functional theory; AFE, antiferroelectric.

*Present address: 241 Jack East Brown Engineering Building, 3122, Texas A&M University, College Station, TX 77843-3122.

†To whom correspondence should be addressed. E-mail: wag@wag.caltech.edu.

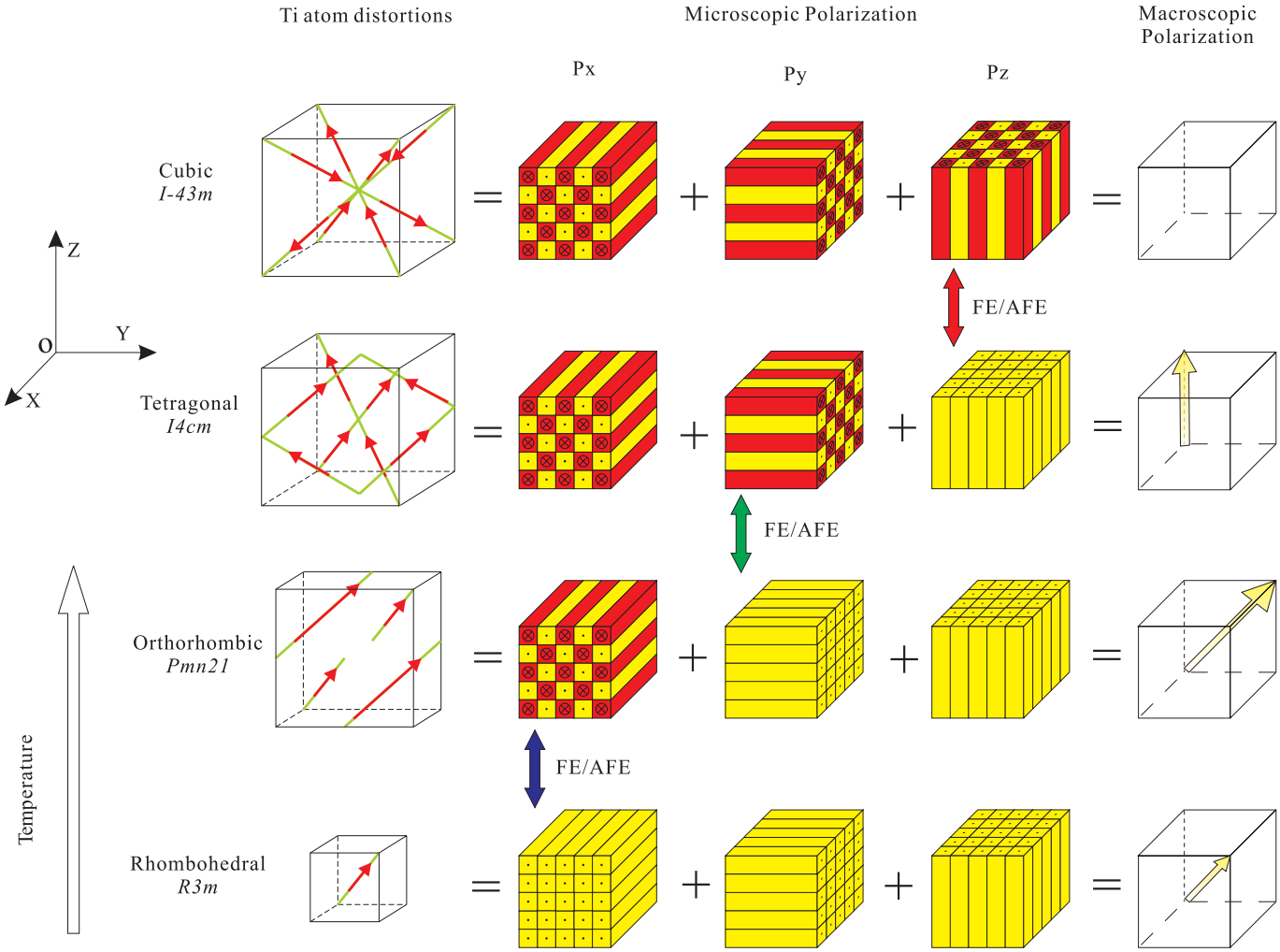

Fig. 1. Ti atom distortions and polarizations determined from QM calculations. Ti distortions are shown in the FE–AFE fundamental unit cells. Yellow strips represent individual Ti-O chains with positive polarization, whereas red indicates negative polarization. The low temperature R phase has FE coupling in all three directions, leading to a net polarization along the ⟨111⟩ direction. Increasing temperature leads to a series of FE to AFE transitions, with macroscopic polarization that switches from ⟨111⟩ to ⟨011⟩ to ⟨001⟩ and then vanishes.

present even in the paraelectric phase far above Tc. These correlations were also discovered in a MD study (24) using the nonlinear oxygen polarizability model.

Despite all these progresses, the ground-state structures of the high-temperature phases were not identified in the previous studies. Knowing the ground-state structures is necessary to obtain an accurate description of domains, interface, and vacancies.

Results and Discussion

We report here QM calculations using the PW91 (25) generalized gradient approximation flavor of DFT. In contrast to previous QM studies, we use unit cells extended to allow the Ti atoms to displace along various ⟨111⟩ directions while retaining the proper macroscopic symmetries. This method leads to the normal ***R3m*** space group for the R phase, ***Pmn21*** for the O phase (this was ***Amm2*** in the displacive model), ***I4 cm*** for the T phase (this was ***P4 mm*** in the displacive model), and ***I-43m*** for the C phase (this was ***Pm3m*** in the displacive model). The primitive unit cells have 1, 2, 4, and 4 molecular units for the R, O, T, and C phases (Fig. 1), respectively.

We find that for C, the optimum position of each Ti is displaced by 0.14 Å along the ⟨111⟩ direction, leading to an energy 2.981 kJ/mol lower than if the Ti had been kept in the center of the octahedron (as in previous calculations using a single molecular unit per cell). [Although the average accuracy of PW91/DFT for cohesive energies is only ≈17 kcal/mol (26, 27), we expect much greater accuracy along a reaction path since the distances between the various atoms change little from point to point.] Thus, the extended unit cell for the C phase has antiferroelectric (AFE) couplings in the x, y, and z directions (Fig. 1). The size of the unit cell changes little (increasing by 2% from the ***Pm3m*** cell to the ***I-43m*** cell).

For T, we also find AFE coupling in the x and y directions, with displacements of 0.13 Å and an energy lowering of 0.373 kJ/mol with respect to the ***P4 mm*** cell. In addition, the QM-derived FE–AFE model (space group ***I4 cm***) leads to $c/a = 1.0104$ in excellent agreement with experiment (1.010), whereas assuming the displacive model (space group ***P4 mm***) leads to 1.0419. Thus, the FE–AFE description resolves the difficulty in correctly predicting the c/a ratio, which long plagued the QM calculations (28).

For the O phase, the QM FE–AFE model (***Pmn21***) leads to a displacement of 0.09 Å and an energy lowering of 0.076 kJ/mol with respect to the displacive phase (***Amm2***).

Thus, the QM calculations lead directly to an ordered FE–AFE microscopic structure as the ground state of the O, T, and

C phases. The relative energies of these phases are 0.000 (R), 0.063 (O), 0.561(T), and 1.020(C) kJ/mol per molecular unit. In the FE–AFE phase structures, each Ti atom is displaced along one of the ⟨111⟩ directions in such a way that inside each -(-Ti-O-)$_n$- chain, all Ti atoms are displaced head to tail, whereas adjacent chains are either FE coupled or AFE coupled. In each case FE coupling introduces net polarization, whereas AFE coupling leads to zero macroscopic polarization. In contrast to the displacive structures for O, T, and C, all phonon frequencies are real so that the FE–AFE phase structures are all dynamically stable. We show below that this FE–AFE model derived directly from QM explains all previous inconsistencies with experiment in the properties of $BaTiO_3$.

The Ti-O lattice mode near the zone center is observed to be both IR and Raman active, which is not possible for the displacive model due to the center of inversion. The FE–AFE cubic phase does not have inversion symmetry, allowing both Raman and IR transitions (3), as observed experimentally.

A strong test of the FE–AFE model is for the T phase, where XAFS (4) finds that each titanium atom displaces from its closest ⟨111⟩ direction by 11.7 ± 1.1° toward the *c* axis, whereas the displacive model would lead to 54.7°. The QM for the FE–AFE model predicts that the displacement angle is 10.8°.

The AFE coupling leads to a much softer phonon structure than the FE coupling. Thus the Γ point Ti-O vibration is 239 cm^{-1} for R (three degenerate values), and 60 cm^{-1} for C (three degenerate values). For the O and T phases, there are one and two low-frequency modes, respectively, corresponding to the AFE couplings. These 0 K results agree well with the 400 K experiments: three modes at 63 cm^{-1} for C and two at 55 cm^{-1} for T. In contrast, the displacive model leads to unstable modes (negative eigenvalues in the Hessian) for the C phase (17) and also for T and O. Thus, in the QM-derived FE–AFE model at each phase transition, a high-energy polar mode (>200 cm^{-1}) parallel to the FE coupled chains transforms to a low-energy polar mode (soft mode <100 cm^{-1}) parallel to the AFE coupled chains. Such heavily damped low-energy soft modes have long been observed (5, 10–12).

Our QM calculations of the AFE C phase (using the frozen phonon model) predict a giant volume dependence of the soft mode frequency near the transition. Thus we calculate the soft mode Gruneisen parameter to be

$$-\frac{V}{\omega}\frac{\partial\omega}{\partial V} = -49,$$

showing the stabilization soft mode from volume expansion. This finding is in good agreement with the experimental value of −43 derived from infrared reflectivity measurements (5). This giant volume dependence of the soft mode indicates a strong coupling between the soft mode and the longitudinal acoustic mode at Γ point, leading to a large damping constant near the transition (as observed experimentally in ref. 5, ≈100 cm^{-1}).

These low frequencies for the AFE directions lead to low zero point quantum corrections and large contributions to the entropy changes upon transition. Thus, using the calculated frozen phonon spectrum to evaluate the entropy, we calculate 0.50 J/mol for T to C in excellent agreement with the value of 0.52 from experiment; ref. 29). It is this increase in entropy for the FE to AFE transitions that leads to phase transitions from R to O to T to C with increasing temperature despite the increase in enthalpy. Our DFT calculations lead to lattice parameter of 4.033 Å at 0 K for the C phase, which is 0.5% larger than the experimental value (30) of 4.012 Å at 400 K. This overestimated lattice parameter leads to a higher transition temperature and transition entropies. In addition, we ignored Ti disorder in the polarization directions. This simplification would overestimate the free energy of the C phase more than the free energy of the T phase, leading to an higher transition temperature for T to C (Fig. 2).

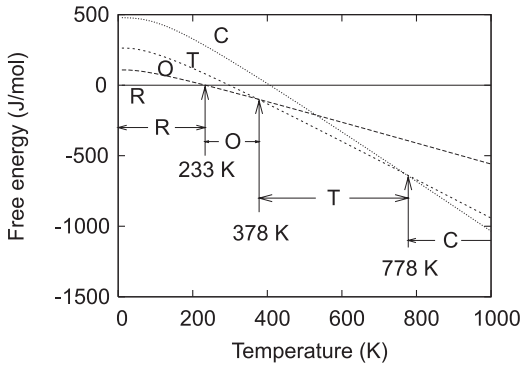

Fig. 2. Free energies predicted for $BaTiO_3$ FE–AFE phase structures. AFE coupling has higher energy but larger entropy than FE coupling. This leads to a series of phase transitions with transition temperatures and entropies of 233 K and 0.677 J/mol (R → O), 378 K and 0.592 J/mol (O → T), and 778 K and 0.496 J/mol (T → C). This finding is comparable with the experimental (29) values of 183 K and 0.17 J/mol (R to O), 278 K and 0.32 J/mol (O to T), and 393 K and 0.52 J/mol (T to C).

Another puzzling property of $BaTiO_3$ has been the diffuse x-ray diffraction (6) observed in the O, T, and C phases (but not R). We find that the soft AFE modes of the QM FE–AFE model leads to x-ray thermal scattering factors (Fig. 3) that explain the observed diffuse lines in experiment (6). Girshberg and Yacoby (31) suggested that the ferroelectric phase transition results from strong intraband electron–phonon interaction, but did not provide underlying atomistic structures to explain the postulated interactions. Chapman *et al.* (32) found that the TA mode is softer than the TO mode for all *k* and the TO mode contribution to diffuse scattering sheets is negligible for $BaTiO_3$. They further suggested that disordering of the local displacements leads to the diffuse scattering.

Our study confirms that the TO mode contribution to sheets in BaTiO3 is negligible. In addition, we found that the diffuse pattern is caused by the anisotropic soft TA mode. In the following, we show that the TA mode is always softer than the TO mode due to the symmetry reduction in $BaTiO_3$ The TA mode in the cubic phase (***I-43m*** in the FE–AFE model) is closely related to the soft TO mode in the simple cubic phase (***Pm3m***). To show this relation, we constructed a series of intermediate phase structures between ***Pm3m*** and ***I-43m***. Each transitional phase structure is given by

$$X = (1 - L)X_{Pm3m} + LX_{I\text{-}43m},$$

where *X* is the lattice parameter or atom fractional coordinates, and *L* ranges from 0 (leading to ***Pm3m***) to 1 (leading to ***I-43m***). Then, we calculated the phonon dispersion of TO and TA modes as a function of *L*. Fig. 4 shows the phonon dispersion variations along Γ-X, Γ–M, and Γ–R during the symmetry reduction. Certain TO modes in ***Pm3m*** for BaTiO3 transform to soft TA modes in ***I-43m***. Along Γ–X, the two TO modes in ***Pm3m*** transform into two TA modes in ***I-43m*** (Fig. 4*A*). Along Γ–M, one soft TO mode in ***Pm3m*** transforms into one TA in ***I-43m*** and the hard TO mode with higher frequency remains a TO mode of ***I-43m*** (Fig. 4*B*). Along Γ–G, the two TO modes in ***Pm3m*** are not soft and they remain TO modes in ***I-43m*** (Fig. 4*C*). After these mode transformations, TA modes are always softer than TO modes for all *k* points.

Furthermore, we project the eigenvectors of the TA and TO modes in ***I-43m*** to the TA and TO modes in ***Pm3m***. Thus, we define

PHYSICS

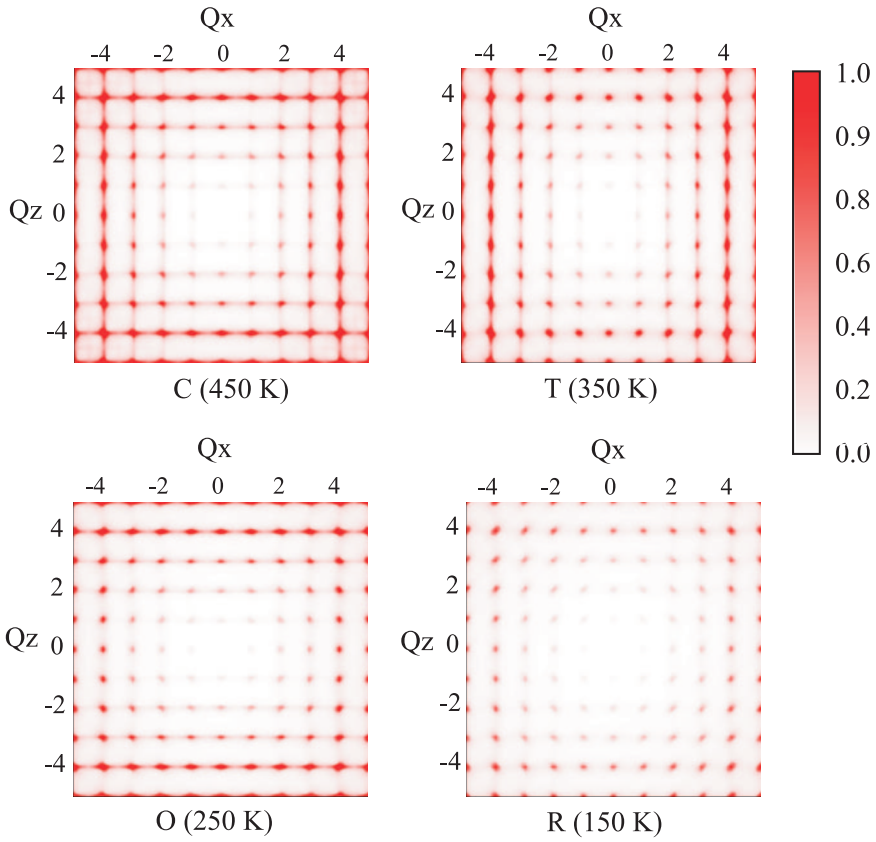

Fig. 3. Diffuse x-ray diffraction predicted from the $BaTiO_3$ FE–AFE phases. The partial differential cross sections (arbitrary units) of x-ray thermal scattering were calculated in the (010) reciprocal plane with polarization vector along [001] for T, [110] for O, and [111] for R. Soft phonon modes cause strong inelastic diffraction, leading to diffuse lines in the pattern (vertical and horizontal for C, vertical for T, horizontal for O, and none for R), in excellent agreement with experiment (6).

$$C_{i,j}(Q) \equiv |\langle \mathbf{e}_{I\text{-}43m}(Q, i)|\mathbf{e}_{Pm3m}(Q, j)\rangle|^2,$$

where **e** is the phonon eigenvector, Q is the wave vector, and I, j = TO or TA. Fig. 5 below shows clearly that the TA mode in ***I-43m*** is related to the TO mode of ***Pm3m***; the major vibration of TA mode in ***I-43m*** is the soft Ti-O motion. By this TO-to-TA transformation, the TA mode picks up soft Ti-O vibrations, leading to lower energy than the TO mode. Because the TO mode in ***Pm3m*** is quite anisotropic (18), the TA mode in ***I-43m*** is very anisotropic due to this TO-to-TA transformation. Thus, it is the anisotropic soft TA mode that leads to diffuse scattering in $BaTO_3$. This finding agrees with the synchrotron radiation experiment of Takesue *et al.* (33).

The I-43m symmetries give the diffraction peaks at $(h/2, k/2, l/2)$ if $h + k + l$ = even. This observation leads to additional Bragg peaks at the face centers of the reciprocal lattice of Pm3m. However, because the atomic distortions from ***Pm3m*** to ***I-43m*** in $BaTiO_3$ are small (≈0.14 Å), the intensities of these additional points are very weak. The maximum intensity of the additional points in the (001) zone is only 0.025% of the (400) intensity (See Table 1, which is published as supporting information on the PNAS web site). These weak Bragg points are further obscured by the background of thermal diffuse scattering. Nevertheless, it should be possible to eventually refine the experiments to test the QM predictions.

The electric field gradient analysis of the NMR experiments (34, 35) for T leads to distortions along ⟨100⟩, in disagreement with the analysis of XAFS experiments (4), which indicate that all Ti distort nearly along ⟨111⟩ directions. Stern (36) has explained that this difference arises from the time averaging implicit in the NMR, so that the correct instantaneous structure is in the ⟨111⟩ direction found in XAFS (4) and now in QM. The AFE coupling has softer TO modes than the FE coupling, leading to diffuse x-ray scattering and phase transitions. Each AFE coupling is doubly degenerate, $\uparrow\downarrow\uparrow\downarrow\ldots\ \uparrow\downarrow$ and $\downarrow\uparrow\downarrow\uparrow\ldots\downarrow\uparrow$. The transition between the two states involves a soft TO mode (<200 cm^{-1}) at the zone boundary. The transition time between the two states is longer than that of XAFS but shorter than that for NMR, leading to ⟨111⟩ detection from XAFS and ⟨001⟩ in the tetragonal phase from NMR. In contrast, the transition between two FE coupling states, $\uparrow\uparrow\uparrow\uparrow\ldots\uparrow\uparrow$ and $\downarrow\downarrow\downarrow\downarrow\ldots\downarrow\downarrow$, requires excitation of a LO mode (≈700 cm^{-1}), which is much more difficult. This giant LO–TO splitting results from the large Born effective charge of Ti as found in the DFT calculations (20).

The QM FE–AFE model leads to many properties qualitatively similar to the 8OD model. The main difference concerns whether adjacent Ti-O chains have AFE coupling or are completely disordered. Our FE–AFE model predicts perfect correlation at the lowest temperatures with a gradual increase in disorder with temperature. In the 8OD model, the entropy increase at each transition would be huge, 5.76 J/mol, in complete disagreement with experiments (29) (0.17–0.52 J/mol). Consequently, the proponents of 8OD make an assumption that there is some correlation length in each chain that greatly reduces the entropy increase. Fitting the 8OD model to experiment requires a very long correlation length of 50–100 Å (8). The FE–AFE leads directly to modest entropy increases at each transition due to the soft phonon structure, without the need for a correlation length assumption.

Our QM calculations show that, for the cubic space group, the ***I-43m*** structure is 2.981 kJ/mol more stable than ***Pm3m***. This

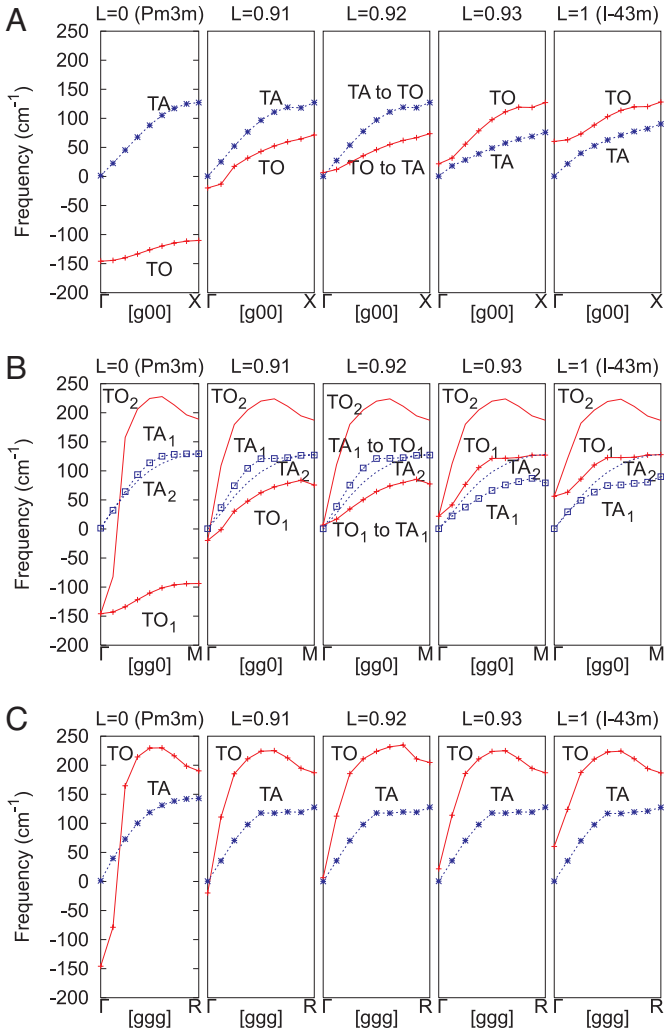

Fig. 4. Calculated phonon dispersions for $BaTiO_3$ cubic phase during the symmetry reduction from *Pm3m* to *I-43m*. (*A*) Two degenerate TO modes transform to two degenerate TA modes along Γ-X at $L = 0.92$. (*B*) One soft TO mode transforms to a soft TA mode along Γ-M. (*C*) No TO-to-TA transformation was found along Γ-R.

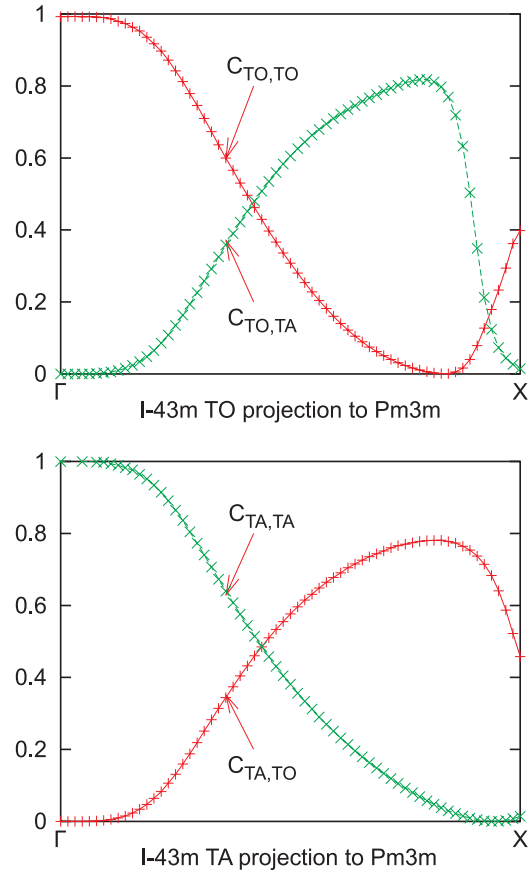

Fig. 5. Projection of the TO and TA modes of *I-43m* to the TO and TA modes of *Pm3m* along Γ-X. The TO modes of *I-43m* have large components of the TA of *Pm3m*. The TA of *I-43m* has a large component of the TO of *Pm3m*. This finding shows that the TA mode of *I-43m* has strong Ti-O motion.

finding shows the importance of the short-range AFE ordering. However, in such calculations, we impose the periodic symmetry of the doubled unit cell; this leaves open the question of whether the AFE ordering is long-range. In the low-temperature rhombohedral ferroelectric phase, it is the strong long-range interactions that keep the local distortions in an ordered pattern. Even above the phase transition temperature, these long-range interactions are expected to be sufficiently strong to retain this ordered pattern characteristic of the lower symmetry group. The difference between long-range interactions and short-range interactions can be illustrated by comparing the frequencies of the LO and TO branches of the same modes. In the ***Pm3m*** phase of $BaTiO_3$, the LO and TO frequencies of the Ti-O interactions were calculated in ref. 37 to be -178 and 738 cm^{-1}. This finding compares to the values of 60 and 751 cm^{-1} that we calculate by using the reduced symmetry, ***I-43m***.

The Girshberg–Yacoby theory (13) emphasizes the interaction between local displacements and phonons, which is consistent with our model: AFE coupling leads to softer phonon structures than FE. Our FE–AFE model provides a fundamental foundation for describing these interactions and can be interpreted within the framework of the Girshberg–Yacoby theory (13).

In summary, our QM studies lead directly to the FE–AFE model for all four phases of $BaTiO_3$ that explains all of the puzzling properties in terms of a competition between the low-energy FE coupling and the high-entropy AFE coupling. These FE–AFE phase structures are the origin of the apparent coexistence of both displacive and order–disorder properties in $BaTiO_3$. Similar behavior has been observed for other perovskite ferroelectrics, such as $KNbO_3$, which we expect will also lead to the FE–AFE model. This new understanding of the fundamental nature of these FE materials should be essential in simulating the dynamical properties of the domain structures important in the macroscopic description of these systems and might be important in optimization the properties of such systems.

Materials and Methods

Our QM calculations (performed with CASTEP 3.8; ref. 38) used the PW91 (25) flavor of DFT, including a generalized gradient approximation for the exchange-correlation interactions. We also used the Vanderbilt-type ultrasoft pseudopotentials (39) for electron–ion interaction and plane wave basis sets (kinetic energy cutoff of 700 eV). The Brillouin zones for the electronic states were sampled by using k points translated from the original $4 \times 4 \times 4$ Monkhorst–Pack (40) mesh for the simple unit cell.

Direct first-principles phonon structure calculations of the FE–AFE cubic phase are expensive and suffer numerical errors in calculating the Hessian. Consequently, we developed the

PHYSICS

PQEq force field (FF) optimized to reproduce the phase structures and energies from the first-principle calculations and then used this FF to calculate the phonon structures. PQEq is an extended shell model (41) using Gaussian shaped shell and core charges (rather than point charges) and including core–core short-range interactions. The dynamic matrices were calculated including the long-wave correction (42, 43) at the Gamma point. For consistency, the phonon Brillouin zone was sampled with Q-points translated from the original $16 \times 16 \times 16$ mesh for the simple unit cell.

The free energy and entropy of each phase were calculated from the phonon density of states (44) using the QM optimized FE–AFE structures (0 K).

The partial differential cross sections were calculated at the level of single-phonon scattering (45) from the phonon structures. The C, T, and O phases were compressed to match their experimental soft mode frequencies (5) at their calculation temperatures. The R phase was compressed to it experimental volume (30). The scattering factors of Ba and O atoms were ignored in these calculations to more clearly identify the physical origin of the diffuse scattering: softer TO modes for AFE coupling than for FE coupling.

This work was initiated with funding by the Army Research Office (ARO, MURI-DAAD19-01-1-0517) and by the National Science Foundation (MRSEC-CSEM-DMR0080065) and completed with funding from Defense Advanced Research Planning Agency (Predicting Real Optimized Materials) through the Office of Naval Research (N00014-02-1-0839). The Molecular Simulation Center computational facilities used in these calculations were provided by grants from Defense University Research Instrumentation Program (DURIP)–ARO, DURIP–Office of Naval Research, and National Science Foundation Major Research Instrumentation.

1. Cochran W (1959) *Phys Rev Lett* 3:412–414.
2. Cochran W (1960) *Adv Phys* 9:387–423.
3. Quittet AM, Lambert M (1973) *Solid State Commun* 12:1053–1055.
4. Ravel B, Stern EA, Vedrinskii RI, Kraizman V (1998) *Ferroelectrics* 206:407–430.
5. Luspin Y, Servoin JL, Gervais F (1980) *J Phys C Solid State* 13:3761–3773.
6. Comes R, Lambert M, Guinier A (1970) *Acta Crystallogr A* 26:244–254.
7. Bersuker IB (1966) *Phys Lett* 20:589–590.
8. Comes R, Lambert M, Guinier A (1968) *Solid State Commun* 6:715–719.
9. Chaves AS, Barreto FCS, Nogueira RA, Zeks B (1976) *Phys Rev B* 13:207–212.
10. Yamada Y, Shirane G, Linz A (1969) *Phys Rev* 177:848–857.
11. Harada J, Axe JD, Shirane (1971) *G Phys Rev B* 4:155–162.
12. Vogt H, Sanjurjo JA, Rossbroich G (1982) *Phys Rev B* 26:5904–5910.
13. Girshberg Y, Yacoby Y (1997) *Solid State Commun* 103:425–430.
14. Pirc R, Blinc R (2004) *Phys Rev B* 70:134107.
15. Cohen RE, Krakauer H (1990) *Phys Rev B* 42:6416–6423.
16. Cohen RE (1992) *Nature* 358:136–138.
17. Ghosez P, Gonze X, Michenaud JP (1998) *Ferroelectrics* 206:205–217.
18. Ghosez P, Cockayne E, Waghmare UV, Rabe KM (1999) *Phys Rev B* 60:836–843.
19. Yu R, Krakauer H (1995) *Phys Rev Lett* 74:4067–4070.
20. Zhong W, Vanderbilt D, Rabe KM (1994) *Phys Rev Lett* 73:1861–1864.
21. Sepliarsky M, Migoni RL, Stachiotti MG (1998) *Comput Mat Sci* 10:51–56.
22. Krakauer H, Yu RC, Wang CZ, Lasota C (1998) *Ferroelectrics* 206:133–155.
23. Krakauer H, Yu RC, Wang CZ, Rabe KM, Waghmare UV (1999) *J Phys Condens Matter* 11:3779–3787.
24. Tinte S, Stachiotti MG, Sepliarsky M, Migoni RL, Rodriguez CO (2000) *Ferroelectrics* 237:345–352.
25. Perdew JP, Chevary JA, Vosko SH, Jackson KA, Pederson MR, Singh DJ, Fiolhais C (1992) *Phys Rev B* 46:6671–6687.
26. Xu X, Goddard WA (2004) *Proc Natl Acad Sci USA* 101:2673–2677.
27. Xu X, Zhang QS, Muller RP, Goddard WA (2005) *J Chem Phys* 122:014105.
28. Uludogan M, Cagin T, Goddard WA (2002) *Mat Res Soc Proc* 718:D10.1.
29. Shirane G, Takeda A (1952) *J Phys Soc Japan* 7:1–4.
30. Kay HF, Vousden P (1949) *Philos Mag* 40:1019–1040.
31. Girshberg Y, Yacoby Y (1999) *J Phys Condens Mater* 11:9807–9822.
32. Chapman BD, Stern EA, Han SW, Cross JO, Seidler GT, Gavrilyatchenko V, Vedrinskii RV, Kraizman VL (2005) *Phys Rev B* 71:020102(R).
33. Takesue N, Maglione M, Chen H (1995) *Phys Rev B* 51:6696–6699.
34. Zalar B, Laguta VV, Blinc R (2003) *Phys Rev Lett* 90:037601.
35. Zalar B, Lebar A, Seliger J, Blinc R, Laguta VV, Itoh M (2005) *Phys Rev B* 71:0064107.
36. Stern EA (2004) *Phys Rev Lett* 93:037601.
37. Zhong W, Kingsmith RD, Vanderbilt D (1994) *Phys Rev Lett* 72:3618–3621.
38. Segall MD, Lindan PJD, Probert MJ, Pickard CJ, Hasnip PJ, Clark SJ, Payne MC (2002) *J Phys Condens Matter* 14:2717–2744.
39. Vanderbilt D (1990) *Phys Rev B* 41:7892–7895.
40. Monkhorst HJ, Pack JD (1976) *Phys Rev B* 13:5188–5192.
41. Dick BG, Overhauser AW (1958) *Phys Rev* 112:90–103.
42. Born M, Huang K (1954) in *Dynamical Theory of Crystal Lattices*, eds Mott NF, Bullard EC (Oxford Univ Press, Oxford), pp 213–277.
43. Cochran W, Cowley RA (1962) *J Phys Chem Solids* 23:447–450.
44. Dove MT (1993) in *Introduction to Lattice Dynamics*, eds Putnis A, Liebermann RC (Cambridge Univ Press, Cambridge, UK), pp 64–65.
45. Lovesey SW (1977) in *Dynamics of Solids and Liquids by Neutron Scattering*, eds Lovesey SW, Springer T (Springer, Heidelberg), pp 22–29.